

Observations and Preliminary Modeling of the Light Curves of Eclipsing Binary Systems NSVS 7322420 and NSVS 5726288

MATTHEW F. KNOTE,^{1,2} RONALD H. KAITCHUCK,² AND ROBERT C. BERRINGTON²¹*Florida Institute of Technology*²*Ball State University*

ABSTRACT

We present new photometric observations of the β Lyrae-type eclipsing binary systems NSVS 7322420 and NSVS 5726288. These observations represent the first multi-band photometry performed on these systems. The light curves were analyzed with PHOEBE, a front-end GUI based on the Wilson-Devinney program, to produce models to describe our observations. Our preliminary solutions indicate that NSVS 7322420 is a primary filling semi-detached system with unusual features warranting further study. These features include a pronounced O'Connell effect, a temporal variance in the light curve, and an unusual “kink” in the light curve around the secondary eclipse. The cause of these features is unknown, but one possibility is the transfer of mass between the component stars. Meanwhile, NSVS 5726288 is probably a typical detached system.

1. INTRODUCTION

Eclipsing binary systems are an important class of variable star as they allow the determination of several characteristics that are otherwise difficult or impossible to determine without resolving the stellar components. Photometric measurements allow the determination of the orbital inclination of the system as well as the shapes and radii of the component stars for totally eclipsing systems, while radial velocity measurements allow the determination of the absolute masses of the components. With both types of measurements, a nearly complete description of the system and its components can be obtained.

We chose two eclipsing binary candidates identified by Hoffman et al. (2008), who identified 409 candidate Algol- and β Lyrae-type eclipsing binary systems in the Northern Sky Variability Survey (NSVS). The NSVS was a survey of the northern sky conducted to record stellar

variations of faint objects (Woźniak et al. 2004). The survey, which was conducted between April 1, 1999 and March 30, 2000 at Los Alamos National Laboratory, imaged 14 million objects north of declination -38° with magnitudes between 8 and 15.5. There were typically a few hundred measurements taken for each object, creating a strong base set for searching for variability. Many systems in the NSVS have not had follow up studies performed due to the enormous volume of data, but works such as Hoffman et al. (2008) have made progress in cataloguing systems based on the NSVS data set itself. The two targets we chose were NSVS 7322420 and NSVS 5726288; details of these two systems and the stars used to analyze them are given in Table 1, while finder charts for the systems are shown in Figure 1. The magnitudes given in Table 1 are taken from the AAVSO Photometric All Sky Survey (APASS) Data Release 9 (Henden et al.

Star	R.A. (J2000)			Dec. (J2000)			B	V	R	I
Designation	h	m	s	d	m	s				
Variable Star										
NSVS 7322420	8	16	12.90	+26	41	13.67	11.675	10.983	10.538	10.122
NSVS 5726288	20	19	11.65	+44	15	47.05	11.607	11.297	11.058	10.831
Comparison Star										
TYC 1936-1001-1	8	17	3.36	+26	45	14.52	11.215	10.695	10.344	10.014
TYC 3163-221-1	20	18	51.80	+44	12	44.81	11.112	10.781	10.549	10.328
Check Star										
TYC 1936-113-1	8	17	5.13	+26	43	6.50	12.228	11.207	10.654	10.139
BD+43 3570	20	19	56.71	+44	11	19.09	11.021	10.894	10.745	10.600

Table 1. List of the designation, coordinates, and B, V, R, and I magnitudes of each variable, comparison, and check star.

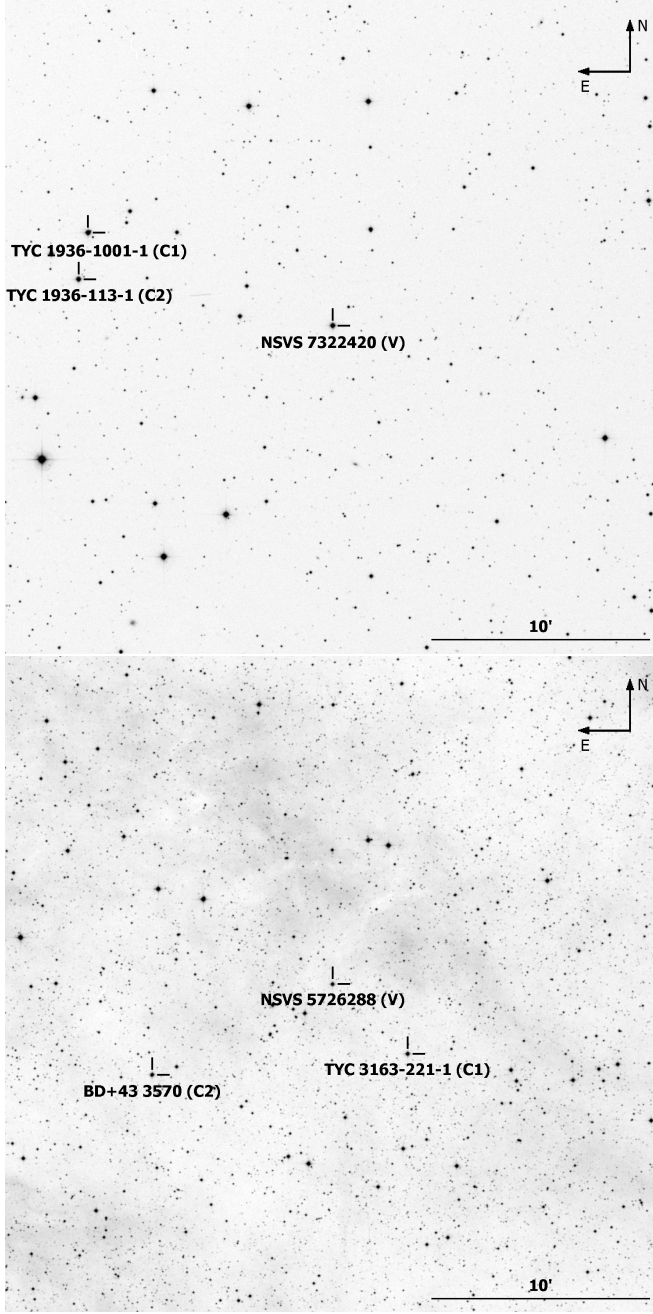


Figure 1. Finder charts for NSVS 7322420 (upper panel) and NSVS 5726288 (lower panel) as well as their comparison stars (labeled C1 and C2).

2016); the Sloan r' and i' magnitudes given by APASS were converted into Cousins R and I magnitudes using transformation equations found in Table 1 of Jester et al. (2005).

Section 2 of this paper describes our acquisition and reduction of the observational data. Section 3 outlines the methods used to analyze our data as well as the results

Target	Observation Date	Telescope	Filters
NSVS 7322420	03/22/2013	BSUO	B, V, R, I
	03/30/2013	BSUO	B, V, R, I
	04/02/2013	BSUO	B, V, R, I
	04/03/2013	BSUO	B, V, R, I
	04/04/2013	BSUO	B, V, R, I
	04/05/2013	BSUO	B, V, R, I
	04/14/2013	BSUO	V, R, I
	04/16/2013	KPNO	V, R, I
	04/21/2013	BSUO	V, R, I
	04/22/2013	BSUO	V, R, I
	04/30/2013	BSUO	B, V, R, I
	05/01/2013	BSUO	B, V, R, I
	05/19/2013	BSUO	B, V, R, I
	05/27/2013	KPNO	B, V, R, I
	11/29/2013	KPNO	B, V, R, I
	01/17/2014	KPNO	B, V, R, I
	01/28/2014	KPNO	B, V, R, I
	01/29/2014	KPNO	B, V, R, I
	10/15/2014	KPNO	B, V, R, I
	10/27/2014	KPNO	B, V, R, I
NSVS 5726288	05/15/2013	BSUO	B, V, R, I
	05/19/2013	BSUO	B, V, R, I
	05/25/2013	BSUO	B, V, R, I
	06/03/2013	BSUO	B, V, R, I
	06/04/2013	BSUO	B, V, R, I
	06/11/2013	BSUO	B, V, R, I
	06/14/2013	BSUO	B, V, R, I
	06/15/2013	BSUO	B, V, R, I
	06/17/2013	BSUO	B, V, R, I
	06/19/2013	BSUO	B, V, R, I
	06/20/2013	BSUO	B, V, R, I
	07/17/2013	BSUO	B, V, R, I
	09/22/2014	BSUO	B, V, R, I
	09/23/2014	BSUO	B, V, R, I
	09/25/2014	BSUO	B, V, R, I
	10/15/2014	KPNO	B, V, R, I
	05/29/2015	BSUO	B, V, R
	11/14/2016	KPNO	B, V, R, I
	11/15/2016	KPNO	B, V, R, I

Table 2. A list of dates of observation along with the location and filters used.

of our analysis. Finally, section 4 contains the discussion of our results as well as details of potential future work.

2. OBSERVATIONS

Our survey of the two systems was conducted between March 2013 and November 2016. We conducted our ob-

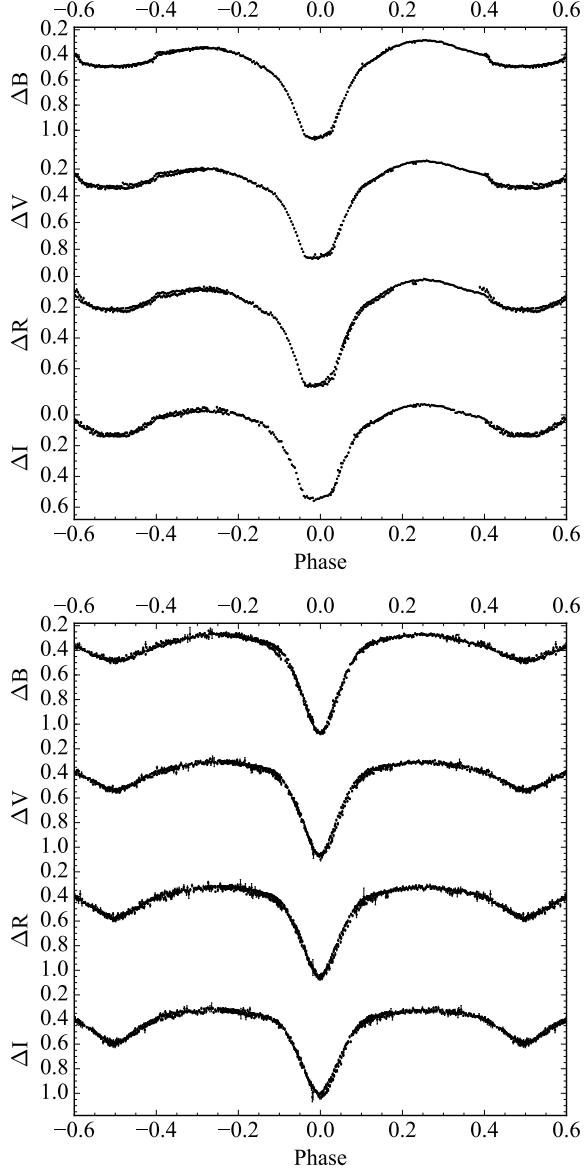


Figure 2. Phased light curves for B, V, R, and I-band data on NSVS 7322420 (upper panel) and NSVS 5726288 (lower panel). Error bars are plotted for all data points. The vertical axis shows the differential magnitude in the given band, while the horizontal axis shows the orbital phase of the system. The data for NSVS 7322420 is only the subset of data taken from January 17, 2014 to January 29, 2014.

servations at two separate sites: the Ball State University Observatory (BSUO) in Muncie, Indiana and Kitt Peak National Observatory (KPNO). The BSUO observations were conducted with a STXL-6303E CCD camera cooled to -10°C mounted on a 16-inch Meade LX200 while the KPNO observations were conducted with a CCD custom built by Astronomical Research Cameras, Inc (ARC) cooled to -110°C mounted on the 0.9-meter SARA-KP

telescope (Keel et al. 2017). Observations were conducted in the Bessell B, V, R, and I filters on all nights excepting brief periods in late April 2013 and May 2015; the Bessell filters (Bessell 1990) closely approximate the Johnson-Cousins photometric system. A list of the nights of observation is presented in Table 2.

Reduction of the obtained images was performed using the CCDRED package contained in the Image Reduction and Analysis Facility (IRAF, Tody 1993). The software AstroImageJ (Collins et al. 2017) was then used to perform photometry on the calibrated images. We used the method of differential photometry to obtain the differential magnitude of our system. The comparison star has a similar color index to the variable so that the two will be similarly affected by atmospheric extinction, although the choice of comparison is limited due to the field of view of our instruments (approximately 15 arcminutes). The comparison star is compared to a check star to ensure that the comparison is non-variable. Once the photometry has been performed, the data is converted to a function of orbital phase (Φ) rather than absolute time using Equations 3 and 4 for NSVS 7322420 and NSVS 5726288, respectively. The phased light curves that were produced and used in our analysis are shown in Figure 2. The unphased standardized magnitude data was uploaded to the AAVSO International Database (Kafka 2015) where it is available for download.

3. ANALYSIS

3.1. Methodology

3.1.1. Ephemeris, period determination, and $O-C$ calculation

The time of minimum for each primary eclipse was calculated using the method described by Kwee & van Woerden (1956). This process was applied to each eclipse in each filter, and the obtained values for each individual eclipse were averaged together to give the reported time of minimum. Period determination was done using the program Peranso (Paunzen & Vanmunster 2016) rather than by examination of the times of minimum light. Peranso allows the user to input a set of observations and use one of a variety of methods to calculate the period. We chose to use the analysis of variance (ANOVA) method described by Schwarzenberg-Czerny (1996). This method, which uses periodic orthogonal polynomials to fit the observed data, excels at detecting and discarding aliases of the true period.

The observed times of minimum light were then compared to a calculated time of minimum. This calculated value for the n^{th} epoch is found using the equation:

$$T_{\text{cal},n} = T_{\text{obs},0} + E_n P \quad (1)$$

Target	Epoch	Time of Minimum (HJD)		O–C (days)
		Observed	Calculated	
NSVS 7322420	0	2456413.632618 ± 0.000201	—	0 ± 0.000201
	454	2456625.861477 ± 0.000027	2456625.862636 ± 0.000201	-0.001159 ± 0.000203
	559	2456674.944067 ± 0.000100	2456674.946671 ± 0.000201	-0.002604 ± 0.000225
NSVS 5726288	0	2456457.738889 ± 0.000178	—	0 ± 0.000178
	543	2456922.677753 ± 0.000231	2456922.685354 ± 0.000178	-0.007601 ± 0.000292
	570	2456945.796265 ± 0.000127	2456945.804239 ± 0.000178	-0.007974 ± 0.000219

Table 3. O–C and observed and calculated times of primary minimum for NSVS 7322420 and NSVS 5726288.

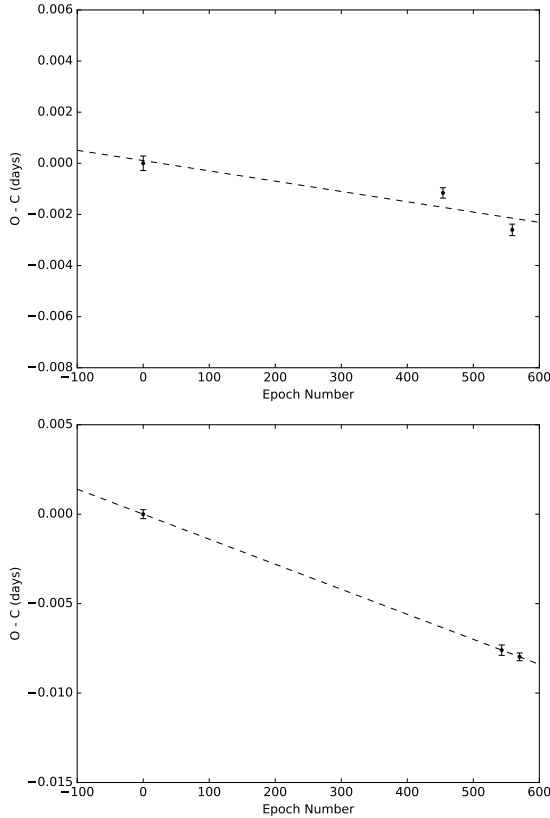


Figure 3. Observed minus calculated (O – C) times of minimum light for NSVS 7322420 (upper panel) and NSVS 5726288 (lower panel) plotted against epoch number. The dashed lines indicate the best linear fit to the data.

where $T_{\text{obs},0}$ is an observed reference time of minimum, E_n is the number of periods elapsed since $T_{\text{obs},0}$, and P is the orbital period. The calculated value was then obtained by subtracting it from the corresponding observed value to obtain O–C. The error in O–C is given by the equation:

$$\sigma_{\text{O–C},n} = \sqrt{\sigma_{T_{\text{obs},n}}^2 + \sigma_{T_{\text{obs},0}}^2} \quad (2)$$

where σ denotes the error of the subscripted parameter.

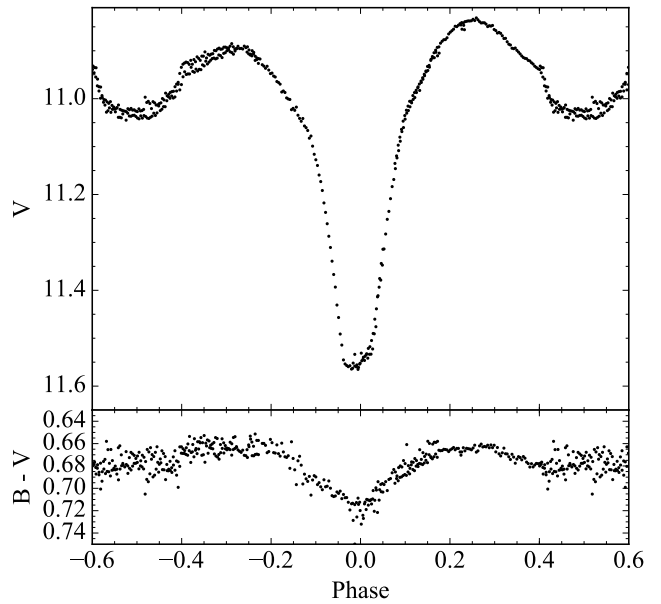


Figure 4. (B–V) color curve for NSVS 7322420. The apparent V-band magnitude is plotted in the top panel, while the (B–V) color curve is plotted in the lower panel. Error bars are not plotted for clarity.

3.1.2. Magnitude calibration

The output file generated by AstroImageJ gives the brightness of the system in relative flux, from which the differential magnitude can be calculated. Estimating the temperature of the stellar components, however, requires the apparent magnitude of the system. The apparent magnitude was obtained by adding the calibrated apparent magnitude of the comparison star given by [Henden et al. \(2016\)](#) to the differential magnitude obtained from AstroImageJ. We performed an analysis to determine the effect the atmosphere had on our determination of the magnitude; we found that the correction factor was negligible and thus our determined magnitude very closely approximates the true apparent magnitude. The error in magnitude was then calculated by adding in quadrature the error in the apparent magnitude of the comparison

Parameter	NSVS 7322420	NSVS 5726288
Orbital Period (d)	0.467467 ± 0.000015	0.856255 ± 0.000007
T_{eff} of Primary Component (K, fixed)	5,700	7,300
T_{eff} of Secondary Component (K)	$3,361 \pm 29$	$5,632 \pm 37$
Orbital Inclination ($^{\circ}$)	91.66 ± 0.04	79.60 ± 0.02
Surface Potential of Primary Component	—	3.1608 ± 0.0035
Surface Potential of Secondary Component	2.6085 ± 0.0088	3.1791 ± 0.0039
Mass Ratio	0.3388 ± 0.0025	0.5789 ± 0.0014
Magnitude Difference ($M_2 - M_1$)	3.4974	1.7431
Spot 1 Temperature (K)	$6,227 \pm 89$	—
Spot 1 Latitude ($^{\circ}$, fixed)	0	—
Spot 1 Longitude ($^{\circ}$, fixed)	90	—
Spot 1 Radius ($^{\circ}$, fixed)	16	—
Spot 2 Temperature (K, fixed)	$6,722 \pm 58$	—
Spot 2 Latitude ($^{\circ}$, fixed)	0	—
Spot 2 Longitude ($^{\circ}$, fixed)	30	—
Spot 2 Radius ($^{\circ}$, fixed)	5	—
Spot 3 Temperature (K, fixed)	$6,722 \pm 58$	—
Spot 3 Latitude ($^{\circ}$, fixed)	0	—
Spot 3 Longitude ($^{\circ}$, fixed)	340	—
Spot 3 Radius ($^{\circ}$, fixed)	5	—

Table 4. Results of the modeling process and analysis for NSVS 7322420 and NSVS 5726288. The errors are the formal errors given by PHOEBE.

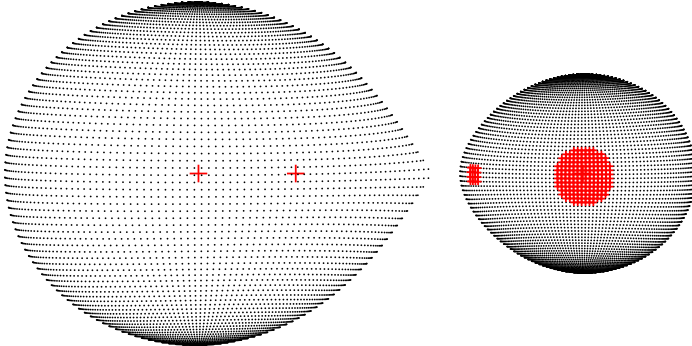


Figure 5. Three-dimensional visualization of the model for NSVS 7322420. The phase of the system in this figure is 0.25, with the primary component on the left and the secondary component on the right; the primary is moving toward the observer. The red markers on the left and right represent the center of each star while the red marker in the center represents the center of mass of the binary system. Two of the three hot spots are clearly visible on the secondary component.

star (also provided by Henden et al.) and the error determined from AstroImageJ. We performed the magnitude calibration and error determination on all data points.

3.1.3. Temperature estimation

A rough estimation for the temperature of the primary component was made by calculating the (B–V) color in-

dex of the system at phase 0.5. Since the observations in the B and V filters did not occur simultaneously, the observational values from the B filter were linearly interpolated to coincide with the values for the V filter. The difference between the interpolated B data and observed V data were then calculated and displayed as a function of phase. These raw values were corrected for interstellar reddening based on the work by Schlafly & Finkbeiner (2011), which provides $E(B-V)$ values for given coordinates based on the assumption that we are observing objects beyond our galaxy. While this assumption does not hold for our stars, this provides a first approximation correction.

Once the corrected (B–V) color curve was obtained, the temperature of the primary component was estimated based upon the (B–V) color index at phase 0.5. At this phase, the primary component mostly or completely obscures the secondary and is therefore the dominant contributor to the observed flux. We used the work presented in Flower (1996) to convert the (B–V) color index at phase 0.5 to temperature under the assumption that the stars are on the main sequence. The secondary temperature was determined through modeling.

3.1.4. Light curve analysis

We used the program PHOEBE (PHysics Of Eclipsing BinariEs) v0.31a (Prša & Zwitter 2005) to analyze

the light curves of the systems and produce a best-fit model. PHOEBE is a graphical user interface built on the Wilson-Devinney (WD) program introduced by [Wilson & Devinney \(1971\)](#). This model includes many parameters that affect the synthetic light curve produced by the program. These parameters are altered using an iterative least-squares analysis known as differential correction to produce the best fit to the observed data.

We input the phased apparent magnitude curves from all four filters into PHOEBE. Data from all filters were fit simultaneously to better constrain the system parameters. The primary temperature was held fixed at the previously estimated value throughout the modeling process while the secondary temperature was allowed to vary. The fact that all of our target stars had temperatures suggesting convective envelopes allowed us to set the gravity brightening and surface albedos to their theoretical values of 0.32 ([Lucy 1967](#)) and 0.5 ([Ruciński 1969](#)), respectively. We performed a mass ratio search (as described in [Qian et al. 2007](#)) to determine the best fit mass ratio.

Following this, we allowed other parameters of the system to vary. These parameters include the Kopal surface potential (Ω), the mass ratio of the system ($q = m_2/m_1$), the orbital inclination (i) of the system, and a phase shift (which was negligible for both systems). Throughout the process, we continued to normalize the luminosities of the component stars and interpolate limb darkening coefficients based on the work by [van Hamme \(1993\)](#). The limb darkening coefficients were interpolated using a logarithmic law as the temperature for all stars is less than 9,000 K.

3.2. NSVS 7322420

Our period analysis for NSVS 7322420 yielded a period of 0.467467 ± 0.000015 days, which is quite close to the value of 0.46740 days published by [Hoffman et al. \(2008\)](#). We determined the average time of minimum on three primary eclipses, and these and the O–C values are listed in Table 3 while a diagram showing the best linear fit to these values is displayed in Figure 3. We used the first time of minimum as the reference minimum, resulting in a linear ephemeris of:

$$T_{\min}(\text{HJD}) = 2456413.6326(2) + 0^d467467(15)E \quad (3)$$

The (B–V) color curve we obtained for this system is shown in Figure 4, from which we estimate a (B–V) color index of 0.68 ± 0.07 during the secondary eclipse (the large error is due to the uncertainty in the apparent magnitudes of the comparison star). [Schlafly & Finkbeiner \(2011\)](#) estimate a $E(B-V)$ of 0.03 at the coordinates of this system, giving a (B–V) color index of 0.65 ± 0.07

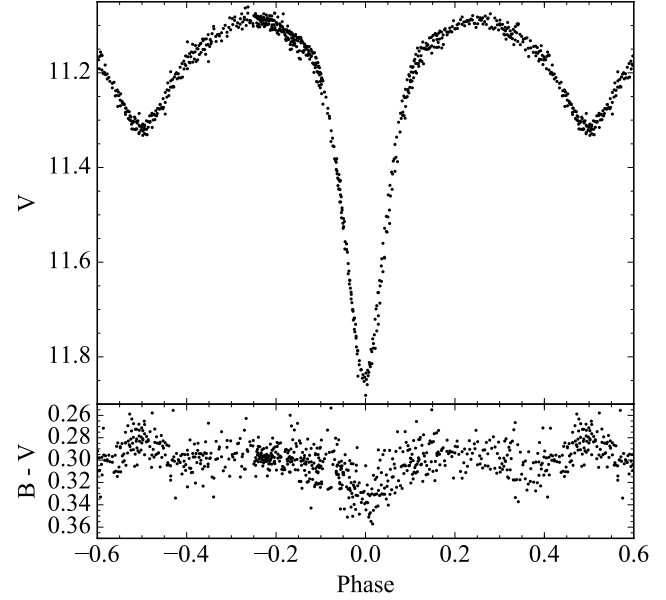


Figure 6. (B–V) color curve for NSVS 5726288. The apparent V-band magnitude is plotted in the top panel, while the (B–V) color curve is plotted in the lower panel. Error bars are not plotted for clarity.

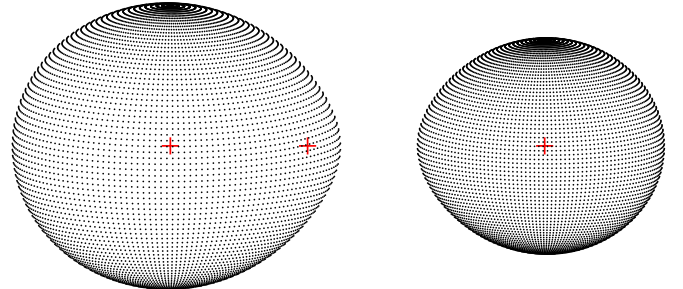


Figure 7. Three-dimensional visualization of the model for NSVS 5726288. The phase of the system in this figure is 0.25, with the primary component on the left and the secondary component on the right; the primary is moving toward the observer. The red markers on the left and right represent the center of each star while the red marker in the center represents the center of mass of the binary system.

during the secondary eclipse. This corresponds to a temperature for the primary component of $5,700 \pm 230$ K and indicates a spectral type of $G3 \pm 3$ ([Fitzgerald 1970](#)).

The system proved difficult to model, due at least in part to the presence of maxima of unequal height: the maximum following primary eclipse is 0.062 magnitudes brighter than the maximum following secondary eclipse in the B band. This is known as the O’Connell effect ([O’Connell 1951, Milone 1968](#)) and may be explained by a hot or cool spot on one of the stars or from gas streams

creating one or more hot spots (Wilsey & Beaky 2009). The model we present matches the observed light curve marginally well, but it is highly artificial as it requires three hot spots in order to adequately explain the observed features in the light curve. While the hot spot located at 90° longitude can be interpreted as the impact of a matter stream onto the stellar surface (Wilsey & Beaky 2009), the two spots located close to 0° longitude have no clear physical interpretation. Spots introduce a considerable amount of degeneracy into the solution, and only the temperature factor of the first spot could be allowed to vary without the program diverging. As a result of these factors, this model should not be interpreted as a completely accurate physical description of the system, and while the general system characteristics are most likely accurate, the specific cause of the light curve irregularities is likely not accurately explained by this model.

The model indicates that the system is a primary filling semi-detached system with a secondary component of spectral type M. Details of this model is given in the middle column of Table 4 while a three-dimensional visualization (produced by *Binary Maker 3*, Bradstreet & Steelman 2002) of the model is given in Figure 5. A comparison of the observed data and synthetic light curves is presented in Figure 8.

3.3. NSVS 5726288

Our period analysis for NSVS 5726288 yielded a period of 0.856255 ± 0.000007 days, which differs quite significantly from the value of 0.59935 days published by Hoffman et al. (2008). This 0.59935 day period is almost exactly seven-tenths of our calculated period, indicating that it is likely an alias caused by poor temporal coverage. We determined the average time of minimum on three primary eclipses, and these and the O–C values are listed in Table 3 while a diagram showing the best linear fit to these values is displayed in Figure 3. We used the first time of minimum as the reference minimum, resulting in a linear ephemeris of:

$$T_{\min}(\text{HJD}) = 2456457.738889(178) + 0^d856255(7)E \quad (4)$$

The (B–V) color curve we obtained for this system is shown in Figure 6, from which we estimate a (B–V) color index of 0.28 ± 0.04 during the secondary eclipse. Schlafly & Finkbeiner (2011) estimate a $E(B-V)$ of 1.55 at the coordinates of this system, giving a (B–V) color index of -1.27 ± 0.04 during the secondary eclipse. This gives a non-physical value for the effective temperature, preventing us from using this method to determine an interstellar extinction correction for this system. The reason

for such a large correction is that the system lies in the plane of the Milky Way and is therefore subject to significant extinction. With no better way to determine the reddening of the system, we chose to use the raw color index (0.28 ± 0.04) as a basis for temperature estimation. This corresponds to a temperature of $7,300 \pm 210$ K and indicates a spectral type of $A8 \pm 1$ (Fitzgerald 1970).

A single, well-fitting model was produced for this system, the details of which can be found in the rightmost column of Table 4. The model indicates a detached system with a secondary component of spectral type G. It should be noted that, due to the lack of correction for interstellar extinction, the values for the temperature are a lower bound. A three-dimensional visualization of the model is given in Figure 7 while a comparison of the observed data and synthetic light curves is presented in Figure 9.

4. DISCUSSION

NSVS 7322420 is a semi-detached system with the primary component filling its critical lobe. The system contains a G3 primary and an M secondary, and the model indicates that the stars are of significantly dissimilar mass. The light curve of the system displays a pronounced O’Connell effect and an unusual “kink” as the system enters and exits secondary eclipse. The system is also rapidly evolving, and data taken in 2013 and late 2014 could not be combined with data taken in early 2014 without producing obvious discontinuities that rendered modeling the system impossible. This light curve variability forced us to use only a subset of the data taken on the system that was relatively close temporally. The model produced is artificial and likely does not accurately explain these unusual features; a more sophisticated modeling program may be necessary.

NSVS 5726288 is a rather standard detached system containing two components of dissimilar mass in a moderately inclined orbit. The system contains an A8 primary and an early G secondary. The determined values for the temperature are lower bounds due to the lack of correcting for interstellar extinction, so it is possible that these stars are significantly hotter than our model indicates. The period of 0.856255 days differs significantly from the value published by Hoffman et al. (2008), which is most likely a symptom of poor temporal coverage of the system by the NSVS.

The O’Connell effect observed in NSVS 7322420 is a poorly understood phenomenon. Wilsey & Beaky (2009) describe several ideas regarding the cause of the effect, but they note that none of these ideas can adequately explain all known examples. The most prevalent explanation of the O’Connell effect is that hot or cool spots

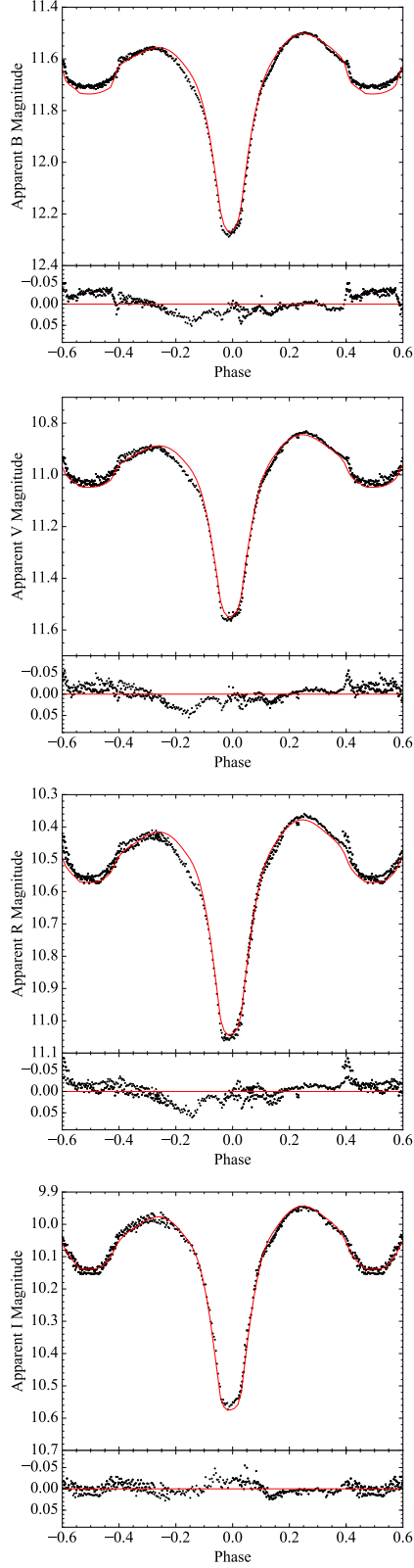


Figure 8. Observed B (top panel), V (second panel), R (third panel), and I (fourth panel) data for NSVS 7322420 plotted against synthetic light curves. The top panel of each figure plots the apparent magnitude of the observed and synthetic light curves against the phase of the system. The residuals for the model are shown in the bottom panel of each figure.

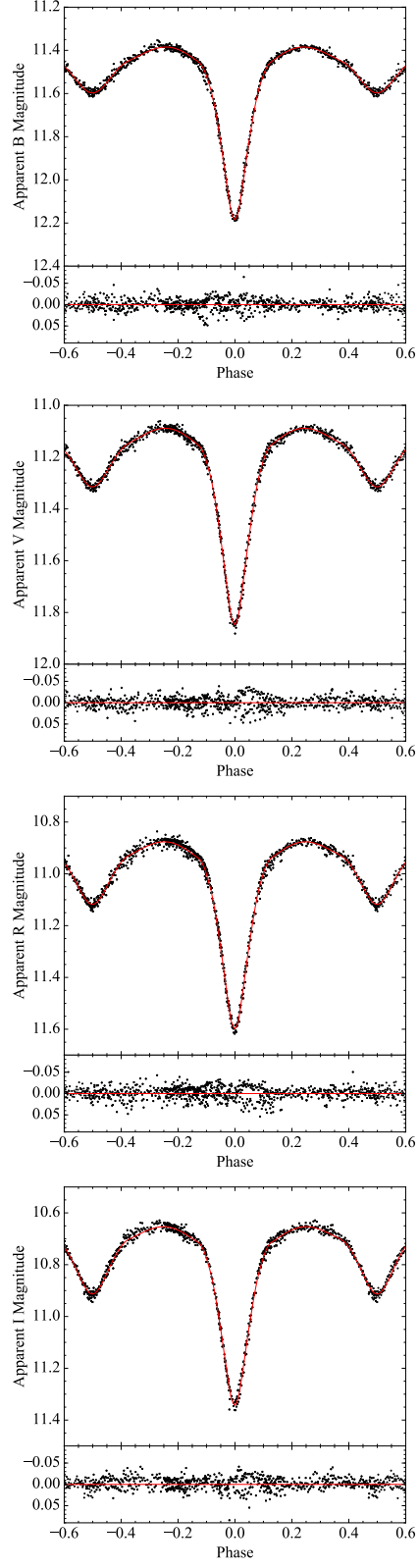


Figure 9. Observed B (top panel), V (second panel), R (third panel), and I (fourth panel) data for NSVS 5726288 plotted against synthetic light curves. The top panel of each figure plots the apparent magnitude of the observed and synthetic light curves against the phase of the system. The residuals for the model are shown in the bottom panel of each figure.

caused by chromospheric activity on one of the components creates a difference in the observed flux for different hemispheres of the star. However, the spots may need to be unrealistically large in size in order to fully describe the observed O'Connell effect, and spots also suffer from the ability to explain almost any deviation from a synthetic light curve if placed correctly, which reduces confidence in the reliability of such models. Furthermore, [Drake et al. \(2014\)](#) finds “no evidence for changes in the maxima that are expected as star spot numbers or sizes vary,” further diminishing the theory that star spots are the cause of the O'Connell effect. An alternate hypothesis proposed by [Liu & Yang \(2003\)](#) suggests that the effect is caused by material surrounding the stars impacting the components as they orbit, resulting in heating of the leading hemispheres. At this time, however, we lack the observational evidence to suggest a plausible source for such material in NSVS 7322420, and we consider it unlikely to explain the effect in the system.

Another hypothesis proposes that the asymmetry in observed flux is caused by a hot spot created by the impact of a matter stream on either the stellar surface or on a circumstellar accretion disk. This hypothesis has been used to explain the O'Connell effect observed in GR Tauri ([Gu et al. 2004](#)), a system that exhibits light curve variability similar to what we observed in NSVS 7322420. Due to this and the previously mentioned irregularities in the light curve of the system (including an asymmetric primary minimum similar to RY Scuti, a system that was modeled with an accretion disk by [Djurašević et al. 2008](#)), we believe that the mass transfer theory represents the most likely explanation of the O'Connell effect in NSVS 7322420.

Unfortunately, photometry alone cannot provide a full description of these systems. Radial velocity data obtained from spectra of these systems would allow us to determine the absolute masses of the components, and therefore the absolute sizes and luminosities of the stars. Spectroscopic data would also provide a direct way to measure the temperatures of the components, which would further refine the parameters of the models. Finally, spectroscopic analysis of NSVS 7322420 could provide clues as to the cause of the unusual features seen in its light curve. Further photometric and spectroscopic observations are being conducted on NSVS 7322420 and will be described in a future paper. The system is also serving as an archetype for a study of systems suspected of undergoing mass transfer.

5. ACKNOWLEDGEMENTS

We would like to thank Drs. Eric Perlman and Saida Caballero-Nieves of FIT for their comments and sugges-

tions regarding this paper. We would also like to thank the Indiana Space Grant Consortium, which partially funded this research project. This paper is based on observations obtained with the SARA Observatory 0.9-meter telescope at Kitt Peak, which is owned and operated by the Southeastern Association for Research in Astronomy ([saraobservatory.org](#)). The authors are honored to be permitted to conduct astronomical research on Iolkam Du'ag (Kitt Peak), a mountain with particular significance to the Tohono O'odham Nation.

REFERENCES

Bessell, M. S. 1990, PASP, 102, 1181

Bradstreet, D. H., & Steelman, D. P. 2002, in Bulletin of the American Astronomical Society, Vol. 34, American Astronomical Society Meeting Abstracts, 1224

Collins, K. A., Kielkopf, J. F., Stassun, K. G., & Hessman, F. V. 2017, AJ, 153, 77

Djurašević, G., Vince, I., & Atanacković, O. 2008, AJ, 136, 767

Drake, A. J., Graham, M. J., Djorgovski, S. G., et al. 2014, ApJS, 213, 9

Fitzgerald, M. P. 1970, A&A, 4, 234

Flower, P. J. 1996, ApJ, 469, 355

Gu, S.-h., Chen, P.-s., Choy, Y.-k., et al. 2004, A&A, 423, 607

Henden, A. A., Templeton, M., Terrell, D., et al. 2016, VizieR Online Data Catalog, II/336

Hoffman, D. I., Harrison, T. E., Coughlin, J. L., et al. 2008, AJ, 136, 1067

Jester, S., Schneider, D. P., Richards, G. T., et al. 2005, AJ, 130, 873

Kafka, S. 2015, Observations from the AAVSO International Database, <https://www.aavso.org/aavso-international-database>

Keel, W. C., Oswalt, T., Mack, P., et al. 2017, PASP, 129, 015002

Kwee, K. K., & van Woerden, H. 1956, BAN, 12, 327

Liu, Q.-Y., & Yang, Y.-L. 2003, ChJA&A, 3, 142

Lucy, L. B. 1967, ZA, 65, 89

Milone, E. E. 1968, AJ, 73, 708

O'Connell, D. J. K. 1951, Publications of the Riverview College Observatory, 2, 85

Paunzen, E., & Vanmunster, T. 2016, Astronomische Nachrichten, 337, 239

Prša, A., & Zwitter, T. 2005, ApJ, 628, 426

Qian, S.-B., Yuan, J.-Z., Soonthornthum, B., et al. 2007, ApJ, 671, 811

Ruciński, S. M. 1969, AcA, 19, 245

Schlafly, E. F., & Finkbeiner, D. P. 2011, ApJ, 737, 103

Schwarzenberg-Czerny, A. 1996, ApJL, 460, L107

Tody, D. 1993, in Astronomical Society of the Pacific Conference Series, Vol. 52, Astronomical Data Analysis Software and Systems II, ed. R. J. Hanisch, R. J. V. Brissenden, & J. Barnes, 173

van Hamme, W. 1993, AJ, 106, 2096

Wilsey, N. J., & Beaky, M. M. 2009, Society for Astronomical Sciences Annual Symposium, 28, 107

Wilson, R. E., & Devinney, E. J. 1971, ApJ, 166, 605

Woźniak, P. R., Vestrand, W. T., Akerlof, C. W., et al. 2004, AJ, 127, 2436